Fatigue damage assessment of a large rail-cum-road steel truss-arch bridge using structural health monitoring dynamic data

Case Studies in Construction Materials 21 (2024) e03772

Contents lists available at ScienceDirect

Case Studies in Construction Materials

journal homepage: www.elsevier.com/locate/cscm

Fatigue damage assessment of a large rail-cum-road steel truss-arch bridge using structural health monitoring dynamic data

Hua-Peng Chen [a,*], Shou-Shan Lu [a,b], Wei-Bin Wu [b], Li Dai [b], Rosario Ceravolo [c]

[a] School of Transportation Engineering, East China Jiaotong University, Jiangxi 330013, China
[b] Jiangxi Transportation Institute Co., Ltd., Nanchang, Jiangxi 330020, China
[c] Department of Structural, Geotechnical and Building Engineering (DISEG), Politecnico di Torino, Torino 10129, Italy

ARTICLE INFO

Keywords:
Rail-cum-road bridge
Structural health monitoring
Finite element modelling
Model updating
Fatigue assessment

ABSTRACT

Structural health monitoring (SHM) system provides valuable information for the fatigue assessment of existing rail-cum-road bridges. This paper aims to develop an effective fatigue assessment approach for the rail-cum-road bridge, Jiujiang Yangtze River Bridge, by utilising the SHM data, focusing on dynamic modal analysis, finite element model updating and fatigue assessment. First, the traffic load spectrum and modal characteristics of the bridge are investigated from the SHM data. A three-dimensional finite element model is constructed and then updated by using the measured modal data through the proposed regularised model updating method. Then, the updated numerical model is verified with the measured dynamic response data, which can be utilised for calculating stress response at critical structural components of the rail-cum-road bridge. Finally, an improved Corten-Dolan's model is proposed to analyse the fatigue damage and structural reliability of the critical structural components of the bridge, taking into account the combined effects of train and highway vehicle loads. The results demonstrate that the proposed fatigue assessment method provides more reliable results for the rail-cum-road bridge by considering the combined effect of multi-level traffic loads and the non-linear fatigue damage accumulation. It is concluded that the short H-shaped suspender is identified as the most vulnerable structural member of the rail-cum-road bridge, and the remaining fatigue service life of the typical components of the bridge should meet the design requirement.

1. Introduction

Rail-cum-road bridges play a crucial role in regional highway and railway transportation links. During the life time service, the bridges are usually subjected to various adverse factors, such as earthquakes, typhoons, corrosion, fatigue, overloading, material ageing, etc. These factors may cause unavoidable structural damage and performance deterioration, leading to safety and durability problems during the service of the bridges [1]. Therefore, a Structural Health Monitoring (SHM) system is necessary to analyse the real-time performance of the rail-cum-road bridge to ensure safe operation [2].

The SHM system provides valuable information for structural performance assessment and maintenance strategy decision-making. The SHM systems have been widely used on long-span bridges in China [3], such as Tsing Ma Bridge [4], Tongling Yangtze River Bridge and Dashengguan Yangtze River Bridge [5]. The SHM data, such as traffic volume, displacements, strain and accelerations, can

* Corresponding author.
E-mail addresses: hp.chen@ecjtu.edu.cn, hp.chen@outlook.com (H.-P. Chen).

https://doi.org/10.1016/j.cscm.2024.e03772
Received 30 January 2024; Received in revised form 29 August 2024; Accepted 15 September 2024
Available online 16 September 2024

be adopted for structural performance analyses, fatigue evaluation and operational modal analyses [6]. From operational modal analyses, the modal properties, such as natural frequencies and mode shapes, can be utilised for updating the associated finite element model.

In general, the finite element model can be constructed based on the design information of the actually built bridge. However, significant discrepancies in structural response and modal parameters may occur between the simulation results and measured results [7]. Recently, many studies on finite element model updating have been undertaken by using measured modal data, such as sensitivity analyses method [8], dynamic perturbation method [9–13] and Bayesian updating method [14,15]. There is still a challenge for updating large-scale complex structures, such as the rail-cum-road bridges, by using the limited information available on the measured modal data. Furthermore, limited studies are available on how the measured structural response under traffic load, such as stress and deflection, are adopted to verify the predictions of the updated numerical model.

For the existing rail-cum-road bridge, fatigue failure often occurs under long-term overload traffic during its service lifetime. Based on the finite element model and SHM data, the fatigue damage of the bridge and its structural components can be analysed and predicted [16]. In the fatigue damage analysis of the rail-cum-road bridge, the highway vehicle loads are often neglected [17–19]. Moreover, the accurate construction of the finite element model is challenging, which can also affects the accuracy of structural performance assessment [20,21]. In the structural performance evaluation, the *S-N* curves such as the Miner's model have been widely used for the bridge fatigue assessment due to the logical relation between stress state and load cycles [22,23], e.g. in bridge structural analysis and designs [24–26]. However, the Miner's model ignores the non-linear characteristics of fatigue damage accumulation and multi-level loading sequence, which may cause considerable errors in fatigue assessment. The Corten-Dolan's model is a useful non-linear fatigue damage cumulative model, which has been widely used in mechanical and aerospace engineering [27]. Investigations have shown that the key exponent parameter in the Corten-Dolan's model depends on many factors, such as material properties and non-linear loading conditions [28], and should be appropriately selected to obtain reasonable prediction results. Recently, studies have been undertaken to modify the exponent parameter [29,30]. However, the Corten-Dolan's model may not be appropriate for applying directly to the rail-cum-road bridge fatigue assessment.

This paper provides an effective fatigue assessment approach for the rail-cum-road bridge based on the SHM data. A three-dimensional finite element model of the rail-cum-road bridge is constructed and then verified by using the proposed regularised

(a)

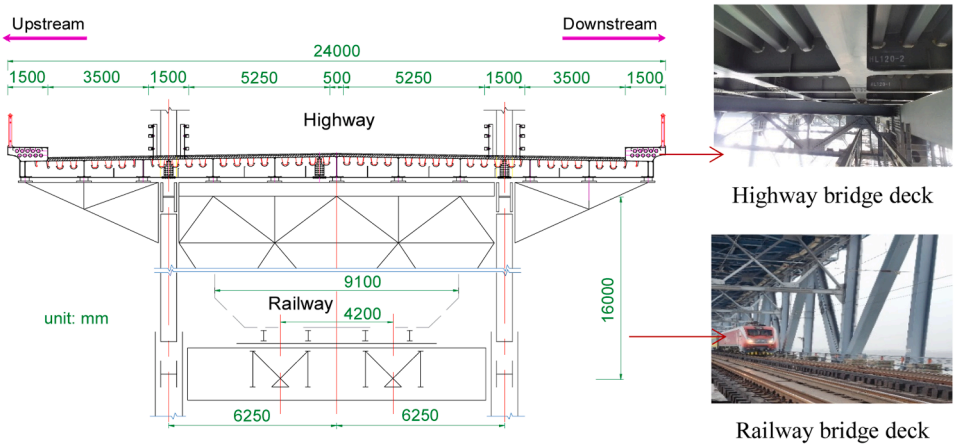

(b)

Fig. 1. The rail-cum-road Jiujiang Yangtze River Bridge: (a) photograph of the bridge; (b) cross-section of bridge decks.

model updating method, based on the identified modal parameters from the vibration data. From the train-bridge coupling analyses, the stress responses of the critical structural components are obtained from the updated numerical model. Finally, an improved Corten-Dolan's model is proposed for bridge fatigue analyses, by considering the coupling effect of the multi-level traffic loads and the nonlinear accumulation of fatigue damage.

2. Bridge characteristics and SHM system

2.1. Bridge description

The construction of the Jiujiang Yangtze River Bridge started in 1973, and it was opened for services in 1993. The rail-cum-road bridge is a steel truss beam and flexible arch bridge for the combined highway and railway transportation, and is located at the boundary of Jiangxi and Hubei provinces in the central region of China. The bridge serves as a crucial transportation node across the Yangtze River, linking the Beijing-Kowloon railway and National Highway G105. The rail-cum-road bridge has a total length of 4,460 m for the highway and 7,675 m for the railway, respectively. The main bridge consists of 3 continuous steel arches with a total span of 576 m (180 m+216 m +180 m), as shown in Fig. 1. The bridge serves a four-lane highway on the upper deck, and a double-track railway on the lower open deck with a design speed of 60 km/h.

The rail-cum-road bridge has been in service for over 30 years, and the bridge has unavoidably suffered from damage and defects, as illustrated in Fig. 2, due to environmental and load effects, such as temperature, humidity, highway and railway traffic loads. Meanwhile, the bridge has been repaired and restrengthened several times during the service life, and the SHM system was deployed for real-time monitoring to ensure bridge safety operation.

2.2. SHM system

In order to optimise sensor arrangements, the structural failure risk analyses and numerical simulations of the bridge were carried out. From the structural vulnerability analyses, the physical parameters for real-time monitoring were determined, including environmental factors (e.g. temperature and humidity), loading conditions (e.g. traffic load and wind load), structural response (e.g. displacement, strain and acceleration), and structural variations (e.g. prestress in bolts).

Based on the bridge geometric characteristics and structural analyses, a total of 263 sensors of various functions were installed on the Jiujiang Yangtze River Bridge. Fig. 3 shows the deployment of sensors placed on the rail-cum-road bridge. The locations for placing these sensors are chosen at the representative points by considering the existing structural damage and the critical locations predicted by finite element analyses.

3. Monitored data analyses

3.1. Highway traffic load spectrum

Based on the Weigh-in-Motion (WIM) system, the recorded data of vehicle overload and overspeed can be used for traffic management. From the statistical analysis results of the vehicles proportion with different axle numbers, the proportion of two-axle vehicles is 79.94 %, and the proportion of three-axle vehicles, four-axle vehicles, five-axle vehicles, and six-axle vehicles have values of 2.46 %, 2.12 %, 0.28 %, and 15.2 %, respectively.

Fig. 4 shows the statistical analyses results of traffic flow and vehicle weight distribution with various numbers of axles in year 2022. In Fig. 4(a), the traffic volume statistics show apparent fluctuations. The average monthly traffic volume typically exceeds 600,000 vehicles, and the upstream traffic volume is usually higher than the downstream. Fig. 4(b) provides the results for the histogram of vehicle weight with different axle numbers. The results indicate that vehicles with fewer axles have a much higher

Fig. 2. Damage in bridge structural components: (a) bolt fracture; (b) fatigue crack; (c) coating spalling.

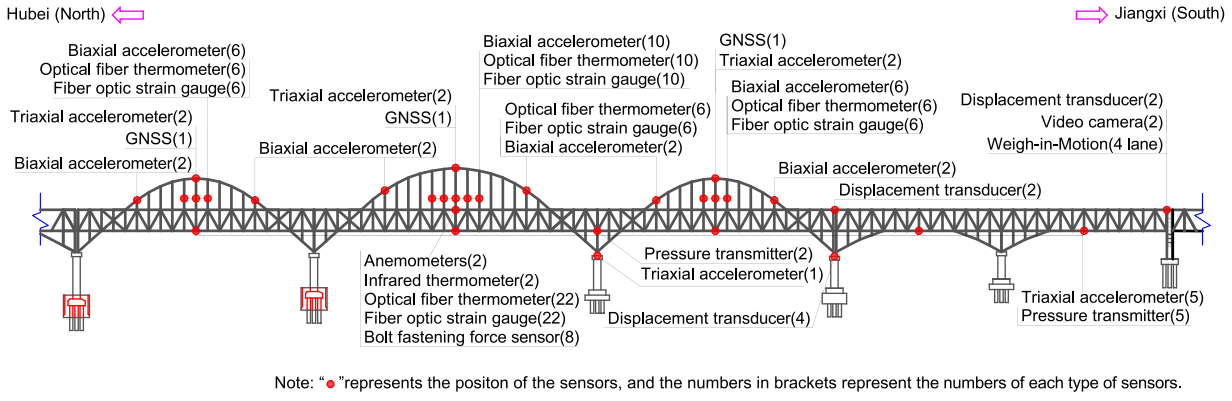

Fig. 3. Instrumentation layout of sensory system for Jiujiang Yangtze River Bridge.

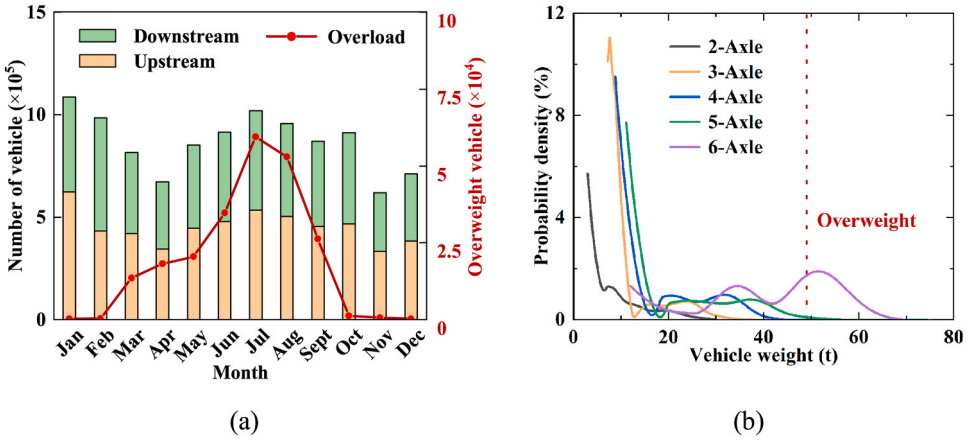

Fig. 4. Traffic statistics in year 2022: (a) traffic flow statistics; (b) vehicle weight (> 3 t only) distributions for different vehicle axle numbers.

proportion of lightweight vehicles, the vehicle weight increases with the number of vehicle axles, and the six-axle vehicles have an overload ratio of 39.2 %.

The probability distribution of traffic characteristics, such as vehicle weight and axle weight, can be modelled by the Gaussian distribution, expressed here as

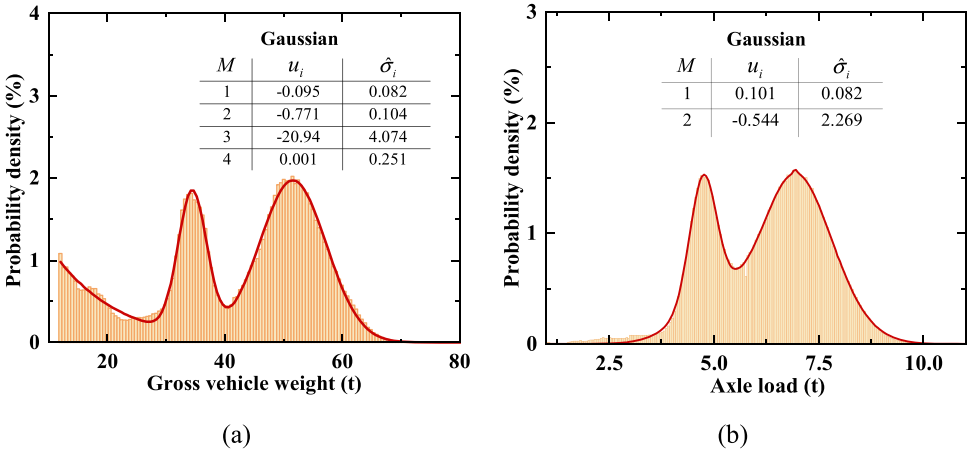

Fig. 5. Probability distributions of gross vehicle weight and vehicle axle weight of six-axle vehicles: (a) gross vehicle weight; (b) axle load of first axle.

$$P = \sum_{i=1}^{M} \lambda_i \exp\left[-\frac{(x - u_i)^2}{2\hat{\sigma}_i^2} \right] \tag{1}$$

where x represents the fitting parameter, such as vehicle weight and axle load; λ_i is the ith ($i = 1, M$) weight coefficient; M is the number of the components of the Gaussian distributions; u_i is the mean value; and $\hat{\sigma}_i$ is the standard deviation of the ith distribution model. The histograms of the vehicle weight and axle load of six-axle vehicles can be fitted with the Gaussian distribution given in Eq. (1), and the multi-peak Gaussian distributions are adopted from the measured traffic data, as shown in Fig. 5.

The representative vehicle load model for fatigue analyses can be obtained based on the statistics of the vehicle weight and axle load. The Miner's model assumes that the total fatigue damage caused by traffic loads can be evaluated by the linear damage accumulation, and neglects the load order effect and non-linear cumulative properties of fatigue damage [20]. Based on the linear damage assumption of the Miner's model, the frequency spectrum of the vehicle loads can be expressed by the equivalent axle load, as shown as

$$W_{ej} = \left[\sum_{i=2}^{B} f_{ij} (W_{ij})^{\hat{m}} \right]^{1/\hat{m}} \tag{2}$$

where B is the axle number of the i-axle vehicle, e.g. $B = 6$ for six-axle vehicle; W_{ij} is the weight of the jth axle of the i-axle vehicle; f_{ij} is the probability of W_{ij}; W_{ej} is the equivalent axle load of the jth axle of the i-axle vehicle; and $\hat{m}$ is the inverse slope of the S-N curve, taken as $\hat{m} = 5$.

The equivalent axle spacing of the jth axle of the i-axle vehicle is given as

$$L_{ej} = \sum_{i=1}^{B-1} f_i L_{ij} \tag{3}$$

where L_{ij} is the axle spacing of the jth axle of the i-axle vehicle; f_i is the probability of L_{ij}; and L_{ej} is the equivalent axle spacing of the jth axle.

Table 1 summarise the representative vehicle fatigue load spectrum. The lightweight vehicles (e.g. gross vehicle weight < 3 t) or vehicles with lower proportion (e.g. proportion < 1 %) can be ignored in bridge fatigue assessment [24]. Although the proportion of two-axle vehicles is 79.5 %, these low-weight vehicles of equivalent weight of 12.6 t have little effect on structural fatigue failure. The proportion of fatigue damage caused by six-axle vehicles and overload vehicles is 98.5 % and 81.1 %, respectively. Thus, the fatigue damage caused by the overloaded vehicles cannot be ignored. The six-axle vehicles cause more significant fatigue damage than overload vehicles due to the larger vehicle number, which could be considered as the typical load model for fatigue assessment.

Table 1
Representative vehicle fatigue load spectrum.

Vehicle type	Vehicle load model, axle load (t), axle spacing (m)	Equivalent weight (t)	Vehicle ratio (%)	Fatigue damage ratio (%)
Two-axle vehicle	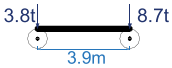	12.6	79.5	0.76
Three-axle vehicle		16.0	2.70	0.09
Four-axle vehicle		23.2	2.30	0.47
Five-axle vehicle	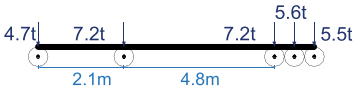	30.1	0.30	0.22
Six-axle vehicle		46.4	15.2	98.5
Overload vehicle (> 49 t)	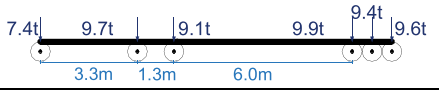	55.1	5.30	81.1

3.2. Operational modal analyses

Modal parameter identification is an essential part of bridge dynamic performance evaluation. Modal parameters, including natural frequencies, can be extracted using the measured ambient vibration data. Fig. 6(a) gives the time history of the acceleration measured by the accelerometer installed at the midspan of the bridge. The natural frequencies of the rail-cum-road bridge can be extracted from the stabilisation diagram by using the data-driven stochastic subspace identification method [1], as shown in Fig. 6(b). From the results, the first eight measured natural frequencies of the Jiujiang Yangtze River Bridge range from 0.57 Hz to 1.51 Hz for various vibration characteristics discussed later in detail.

4. Numerical modelling and model updating

In this paper, a three-dimensional finite element model is adopted to analyse the dynamic behaviour of the rail-cum-road bridge. From the obtained measured modal data, the difference usually exists between the measured and numerical modal data, indicating potential modelling errors in the finite element model and measurement uncertainties from the vibration data. Thus, a finite element model updating procedure is needed to adjust the numerical model by using the measured natural frequencies to improve the correlation between the numerical model and the actual bridge.

4.1. Finite element modelling

Fig. 7 shows the three-dimensional finite element model of the rail-cum-road steel truss arch bridge. In the numerical modelling, the suspenders are modelled with the tensioned truss elements, and the highway bridge deck and other structural components are modelled with beam elements. The elastic modulus of the steel is taken as 210 GPa with a Poisson's ratio of 0.3, and the density of the steel is 7,850 kg/m^3. From the structural characteristics of the bridge, the damping of the bridge is assumed here to be 0.005. The main structural components of the bridge are connected by high-strength bolts, which can be modelled as hinge connection. The constraints between the bridge decks and the upper chords of the main truss are modelled by coupled nodes, and the elastic supports are used to connect the bridge superstructure and foundation. The finite element model has a total number of 44,169 beam elements and 74 tensioned truss elements, with a total number of 4,536 nodes and 10,098 degrees of freedom.

Fig. 8 shows the first six modes obtained from the finite element dynamic analyses. From the results, the fundamental natural frequency is 0.46 Hz with the lateral bending mode shape at the midspan. The first vertical bending mode is observed at the second mode with the natural frequency of 0.61 Hz, and the sixth mode has the natural frequency of 1.22 Hz for antisymmetric bending. The results show that the lateral stiffness of the steel truss arch bridge is much lower than its vertical stiffness. The displacements of the arches and suspenders exist in each mode, indicating that the arches and suspenders are flexible and vulnerable under substantial lateral and vertical loads.

4.2. Model updating

The finite element model has uncertainties in structural parameters, such as stiffness and mass, due to the complexity of the actual bridge, which needs adjustment by using the SHM data. In the model updating process, the updating parameters should be related to the unknown change of structural parameters, such as differences in stiffness $\Delta\mathbf{K}$ and mass $\Delta\mathbf{M}$ between the actual bridge and the associated finite element model.

The dynamic perturbation method provides the exact relationship between the perturbation of structural parameters and modal parameters, and can be used for effective model updating [1]. The global stiffness matrix $\widehat{\mathbf{K}}$ and mass matrix $\widehat{\mathbf{M}}$ of the actual bridge can

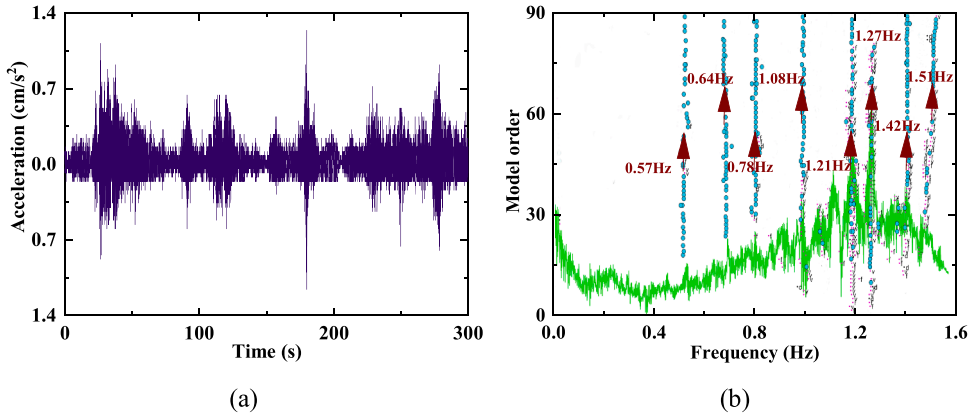

Fig. 6. Operational modal analyses of the bridge: (a) acceleration time-history at mid-span of the bridge; (b) stabilisation diagram of modal identification.

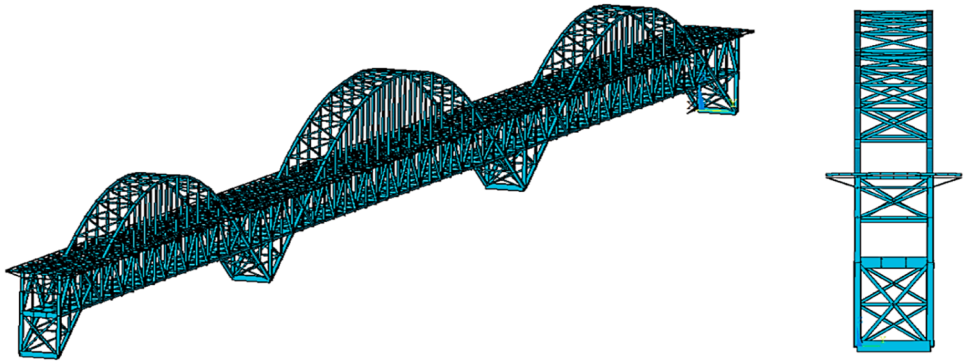

Fig. 7. Finite element modelling of Jiujiang Yangtze River Bridge.

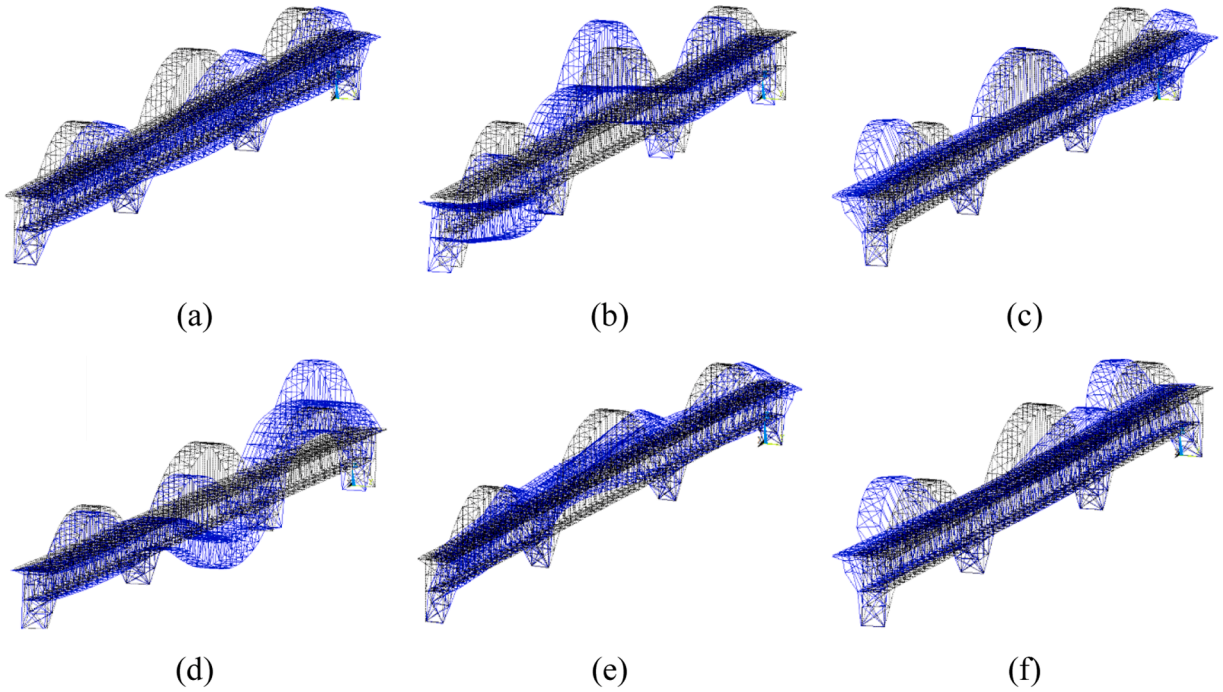

Fig. 8. Numerical natural frequencies and mode shapes of the bridge: (a) mode 1, 0.46 Hz; (b) mode 2, 0.61 Hz; (c) mode 3, 0.63 Hz; (d) mode 4, 1.09 Hz; (e) mode 5, 1.16 Hz; (f) mode 6, 1.22 Hz.

be expressed here as

$$\widehat{\mathbf{K}} = \mathbf{K} + \Delta\mathbf{K}; \widehat{\mathbf{M}} = \mathbf{M} + \Delta\mathbf{M} \tag{4}$$

where **K** and **M** are the global stiffness matrix and global mass matrix of the finite element model, respectively.

For the undamped finite element model and the associated actual bridge, the dynamic characteristic equations can be written, respectively, as

$$\left(\mathbf{K} - \omega_i^2\mathbf{M}\right)\mathbf{\Phi}_i = 0 \tag{5a}$$

$$\left(\widehat{\mathbf{K}} - \widehat{\omega}_i^2\widehat{\mathbf{M}}\right)\widehat{\mathbf{\Phi}}_i = 0 \tag{5b}$$

where ω_i and $\widehat{\omega}_i$ are the ith frequency of the numerical model and the associated actual bridge, respectively; $\mathbf{\Phi}_i$ and $\widehat{\mathbf{\Phi}}_i$are the ith eigenvector of the numerical model and the actual bridge, respectively. It is assumed that the eigenvectors of numerical model are mass normalised to ensure the uniqueness of the eigenvectors.

From Eq. (4) and Eq. (5), The relation between the changes of the structural parameters and the modal parameters can be given as

$$\boldsymbol{\Phi}_i^{\mathrm{T}}\left(\Delta\mathbf{K}-\widehat{\omega}_i^2\Delta\mathbf{M}\right)\widehat{\boldsymbol{\Phi}}_i-\left(\widehat{\omega}_i^2-\omega_i^2\right)\boldsymbol{\Phi}_i^{\mathrm{T}}\mathbf{M}\widehat{\boldsymbol{\Phi}}_i=0 \tag{6}$$

Due to the limited number of sensors adopted typically in the SHM system, the mode shapes of the actual bridge can often be incomplete with few measurements available. Thus, the eigenvectors of the actual bridge could be assumed to remain the same as the corresponding numerical eigenvectors by ignoring the difference between the measured and the numerical eigenvectors. By using the assumed mass normalisation of the numerical eigenvectors, Eq. (6) is rewritten as

$$\boldsymbol{\Phi}_i^{\mathrm{T}}\left(\Delta\mathbf{K}-\widehat{\omega}_i^2\Delta\mathbf{M}\right)\boldsymbol{\Phi}_i=\widehat{\omega}_i^2-\omega_i^2 \tag{7}$$

For model updating, the unknown differences in stiffness and mass between the actual bridge and the numerical model, $\Delta\mathbf{K}$ and $\Delta\mathbf{M}$, can be expressed as

$$\Delta\mathbf{K}=\sum_{j=1}^{N\zeta}\zeta_j\mathbf{K}_j\ ;\ \Delta\mathbf{M}=\sum_{m=1}^{N\eta}\eta_m\mathbf{M}_m \tag{8}$$

where ζ_j and η_m represent the stiffness and mass updating parameters, respectively, which can characterise individual structural elements or element groups, respectively; $N\zeta$ and $N\eta$ are the total number of the stiffness and mass updating parameters, respectively; $\mathbf{K}_j$ and $\mathbf{M}_m$ are the contribution matrices of the jth and mth element or element group to the global stiffness and mass matrices, respectively.

By considering the stiffness and mass updating parameters defined in Eq. (8), Eq. (7) can be rewritten as

$$\sum_{j=1}^{N\zeta}\zeta_j\boldsymbol{\Phi}_i^{\mathrm{T}}\mathbf{K}_j\boldsymbol{\Phi}_i-\widehat{\omega}_i^2\sum_{m=1}^{N\eta}\eta_m\boldsymbol{\Phi}_i^{\mathrm{T}}\mathbf{M}_m\boldsymbol{\Phi}_i=\widehat{\omega}_i^2-\omega_i^2 \tag{9}$$

where the stiffness sensitivity coefficients a_{ij}^{k} and mass sensitivity coefficients a_{ij}^{m} are defined, respectively, as

$$a_{ij}^{\mathrm{k}}=\boldsymbol{\Phi}_i^{\mathrm{T}}\mathbf{K}_j\boldsymbol{\Phi}_i;\ a_{ij}^{\mathrm{m}}=\boldsymbol{\Phi}_i^{\mathrm{T}}\mathbf{M}_j\boldsymbol{\Phi}_i \tag{10}$$

By using the sensitivity coefficients, Eq. (9) can then be simplified as

$$\sum_{j=1}^{N\zeta}a_{ij}^{\mathrm{k}}\zeta_j-\widehat{\omega}_i^2\sum_{m=1}^{N\eta}a_{ij}^{\mathrm{m}}\eta_m=\widehat{\omega}_i^2-\omega_i^2 \tag{11}$$

In order to find a solution for a total number of ($N\zeta$+$N\eta$) stiffness and mass updating parameters, Eq. (11) can be rewritten in a matrix form as

$$\mathbf{A}^{\mathbf{k}}\boldsymbol{\zeta}-\widehat{\boldsymbol{\Omega}}\mathbf{A}^{\mathbf{m}}\boldsymbol{\eta}-\mathbf{f}=0 \tag{12}$$

where $\mathbf{A}^{\mathbf{k}}$ and $\mathbf{A}^{\mathbf{m}}$ are the stiffness and mass sensitivity coefficient matrixes, respectively; $\boldsymbol{\zeta}$ and $\boldsymbol{\eta}$ represent the stiffness and mass updating parameter vectors, respectively; $\widehat{\boldsymbol{\Omega}}$ represent the diagonal matrix of the measured N_m frequencies; and the known vector $\mathbf{f}$ consists of elements $f_i=\widehat{\omega}_i^2-\omega_i^2$, for $i=1, N_m$.

The Tikhonov regularisation is now utilised to obtain a stable solution for the updating parameters to reduce the influence of measurement uncertainty. By using Eq. (12), the solution procedure of the Tikhonov regularisation can be replaced by a constrained optimisation problem as

$$\min\left\{\left\|\mathbf{W}\left(\mathbf{A}^{\mathbf{k}}\boldsymbol{\zeta}-\widehat{\boldsymbol{\Omega}}\mathbf{A}^{\mathbf{m}}\boldsymbol{\eta}-\mathbf{f}\right)\right\|^2+\theta^2\left(\|\boldsymbol{\zeta}\|^2+\|\boldsymbol{\eta}\|^2\right)\right\} \tag{13a}$$

$$\text{Subject to } \zeta_{\mathrm{lb}}<\zeta_j<\zeta_{\mathrm{ub}} \text{ and } \eta_{\mathrm{lb}}<\eta_m<\eta_{\mathrm{ub}} \tag{13b}$$

where $\mathbf{W}$ is the diagonal matrix containing weighting factors to consider the influence and accuracy of the measured frequencies; ζ_{lb} and ζ_{ub} are the lower and upper bounds of stiffness updating parameters, respectively; η_{lb} and η_{ub} are the lower and upper bounds of mass updating parameters, respectively; $\|*\|$ denotes the Euclidean norm; $\theta\,(\theta\geq 0)$ is the Tikhonov regularisation parameter, which can be obtained by the L-curve method [31]. A plot in the log-log scale of the residual norm $p(\theta)$ and solution norm $q(\theta)$ as a function of the regularisation parameter θ is adopted to determine the regularisation parameter, defined as

$$p(\theta)=\left\|\mathbf{W}\left(\mathbf{A}^{\mathbf{k}}\boldsymbol{\zeta}(\theta)-\widehat{\boldsymbol{\Omega}}\mathbf{A}^{\mathbf{m}}\boldsymbol{\eta}(\theta)-\mathbf{f}\right)\right\|^2=\sum_{j=1}^{N\zeta+N\eta}\left[\frac{\theta^2}{\gamma_j^2+\theta^2}\mathbf{u}_j^T\mathbf{f}\right]^2 \tag{14a}$$

$$q(\theta)=\|\boldsymbol{\zeta}(\theta)\|^2+\|\boldsymbol{\eta}(\theta)\|^2=\sum_{j=1}^{N\zeta+N\eta}\left[\frac{\gamma_j}{\gamma_j^2+\theta^2}\mathbf{u}_j^T\mathbf{f}\right]^2 \tag{14b}$$

where γ_j denotes the singular values and the index j range from 1 to $N\zeta$+$N\eta$; and $\mathbf{u}_j$ is the jth orthogonal column vector, which can be

obtained from the singular value decomposition.

Research has shown that the L-curve's corner, where the curvature of the L-curve is approximately maximal, provides an optimal regularisation parameter to balance the residual norm error and the solution norm error [32]. By using the log-log plot of $p(\theta)$ and $q(\theta)$, the curvature value $\kappa(\theta)$ for the L-curve is given by

$$\kappa(\theta) = \frac{2qp}{q'} \frac{\left(\theta^2 q' p + 2\theta qp + \theta^4 qq'\right)}{\left(\theta^4 q^2 + p^2\right)^{3/2}} \tag{15}$$

where q' denotes the first derivative of q. Consequently, the optimal regularisation parameter θ is obtained by maximising the curvature $\kappa(\theta)$.

4.3. Bridge model updating

Structural parameters such as stiffness are often selected for model updating, since stiffness plays a crucial role in finite element modelling. For the complex steel truss arch bridge, it is challenging to adopt a large number of updating parameters representing all structural components, because the number of the bridge structural components is tremendous, and information on the measured modal data is often very limited. Therefore, it is appropriate to group structural components of the same type and update them by using the shared updating parameter.

For the rail-cum-road bridge, a total number of 9 structural components groups are adopted, including the top chords, lower chords, inclined chords, vertical chords, arches, suspenders, highway beams, railway beams, and other components, as shown in Table 2. In each group, a scalar multiplier is employed to represent the updating rate of structural stiffness in Eq. (8), and the mass properties updating procedure is not considered in this paper due to its relatively higher accuracy.

The proposed regularised model updating method is adopted to update the numerical model of the steel truss arch bridge. An optimisation algorithm is utilised to obtain the regularisation parameter from Eq. (15), giving a value of $\theta = 0.432$. Then, a non-linear constrained optimisation method is adopted to find the optimal stiffness updating parameters using Eq. (13a), where the lower and upper bounds of the updating parameters are taken as -20 % and 20 %, respectively, on the basis of the discrepancy between the calculated and measured natural frequencies. Fig. 9 presents the results for the stiffness updating parameters for 9 structural components groups, showing maximum updating rates of less than 10 % for the top chords and vertical chords, and an average absolute updating rate of 5.8 %.

In order to evaluate the performance of the updated finite element model, the average absolute error between the measured frequencies and numerical frequencies for N_m modes are defined as

$$e_{\mathrm{f}} = \frac{1}{N_m} \sum_{i=1}^{N_m} \frac{|\omega_i - \widehat{\omega}_i|}{\widehat{\omega}_i} \tag{16}$$

Table 3 compares the calculated natural frequencies for the original numerical model and updated numerical model with the measured natural frequencies. From the results, the natural frequencies of the updated model are much closer to the measured results. The average absolute relative error e_{f} reduces from 7.91 % before updating to 3.43 % after updating.

4.4. Numerical model verification

Based on the updated finite element model, the structural responses under the traffic load are analysed, and the accuracy of the updated numerical model is verified by comparison with the measured data. To investigate the dynamic response caused by the train load, the spring damping unit is used to simulate the fastener, and the physical parameters of rail track systems listed in Table 4 are adopted [33]. An eight-coach metro train carriage (CR200J) is chosen as the train load model, with a speed of 60 km/h. Typical

Table 2
Structural components groups for model updating.

Group	Type	Components details	Components number
1	Top chords	Top chords of the main truss	128
2	Lower chords	Lower chords of the main truss and stiffening chords	152
3	Inclined chords	Inclined chords of the main truss	152
4	Vertical chords	Vertical chords of the main truss	316
5	Arches	Arch elements	92
6	Suspenders	Suspenders of the arch	74
7	Highway beams	Orthotropic steel bridge decks (modelled as space beams)	1,354
8	Railway beams	Railway longitudinal and cross beams	128
9	Others	Longitudinal and lateral connections of highway deck, top lateral connections of arch, lower lateral connections of railway deck	1,847

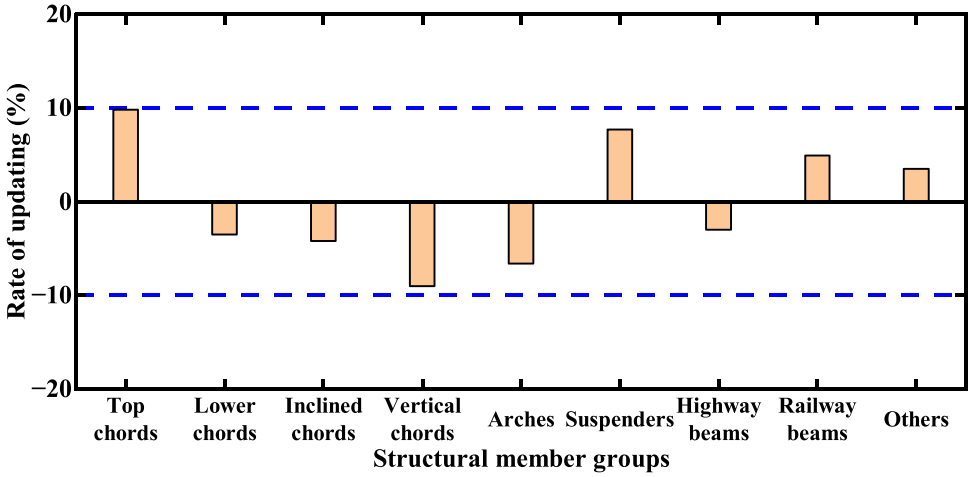

Fig. 9. Updating rates of stiffness parameters for 9 structural member groups.

Table 3
Comparison of calculated frequencies with measured data before and after updating.

Measured $\tilde{\omega}$ (Hz)	Before updating		After updating		Mode description
	Calculated ω (Hz)	Relative error (%)	Calculated ω (Hz)	Relative error (%)	
0.57	0.46	−19.30	0.52	−8.77	Midspan lateral bending
0.64	0.61	−4.69	0.62	−3.13	Side span vertical bending
0.78	0.63	−19.23	0.73	−6.41	Anti-symmetrical bending
1.08	1.09	0.93	1.10	1.85	Side span vertical bending
1.21	1.16	−4.13	1.19	−1.65	Three-span symmetrical bending
1.27	1.22	−3.94	1.26	−0.79	Anti-symmetrical bending
1.42	1.31	−7.75	1.47	3.52	Side span vertical bending
1.51	1.56	3.31	1.53	1.32	Three-span symmetrical bending

Table 4
Physical parameters of rail track systems.

Components	Stiffness (MN/m)	Damping (kN•s/m)	Density (kg/m^3)	Poisson's ratio
Rail	2.1×10^5	-	7800	0.3
Wooden sleeper	1.5×10^4	-	2800	0.3
Fastener	60	72	-	-

railway track spectral characteristics are adopted as random unevenness sources to consider track random irregularity. From updated numerical model, the wheel-rail interaction force is obtained, and the structural dynamic response are analysed when the train pass through the bridge.

Fig. 10 presents the results by comparing the numerical predictions with the corresponding measured data under the train load at the mid-span of the main girder of the second arch structure of the bridge, showing that it takes about 40 seconds for a train to cross the bridge. In Fig. 10(a), the simulated deflection is relatively smooth and regular, and the recorded deflection data has some random fluctuations, which may be caused by the vehicle traffic vibration and noise. Fig. 10(b) presents the comparison of the predicted acceleration time history with the corresponding recorded data. The predicted results from the updated finite element model are generally consistent with the measured data, such as the acceleration magnitude and time range, although there is some difference between the predicted results and measured data. The vibration data measured from the installed accelerometer appear more intensive, indicating that the sampling frequency of the accelerometer is relatively higher. Fig. 10(c) and Fig. 10(d) show the strain response under the train load. There are slight differences between the numerical predictions and the recorded data. Thus, the predicted strain is suitable for bridge fatigue analyses. From the results, the dynamic response predicted by the updated numerical model are well consistent with the measured data. Therefore, the updated finite element model can serve as a benchmark for bridge fatigue assessment.

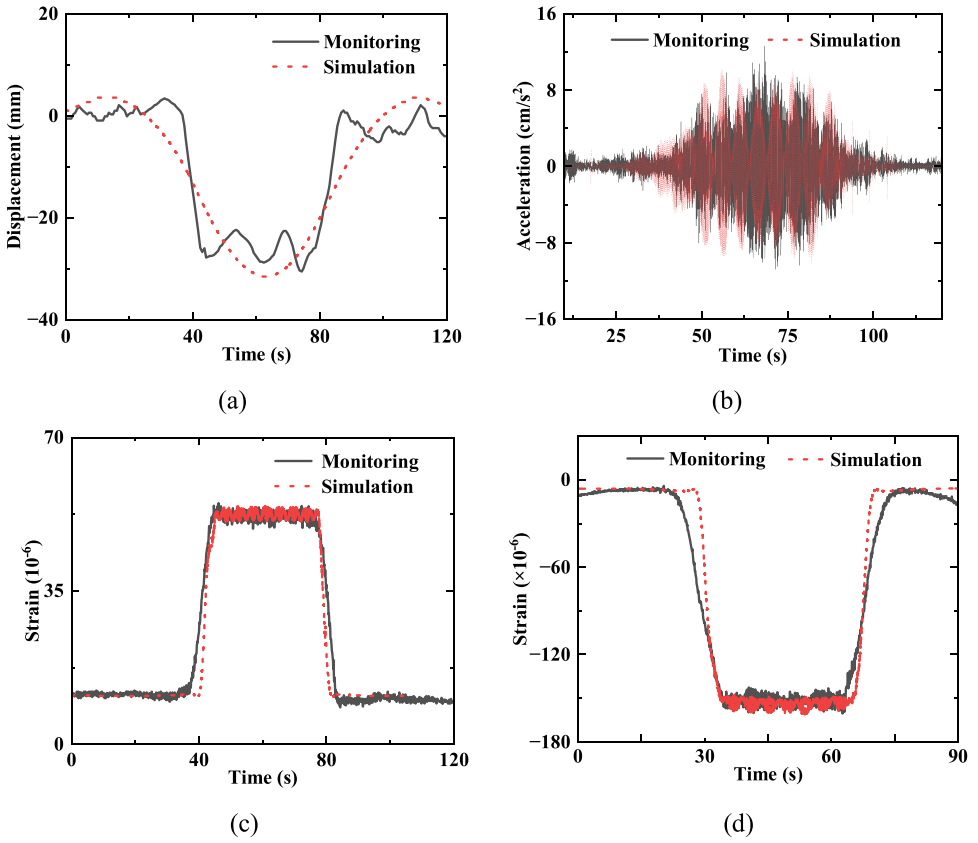

Fig. 10. Comparison of the predicted dynamic response with the corresponding measured data at train speed of 60 km/h: (a) vertical displacement at mid-span; (b) vertical acceleration at the mid-span; (c) strain in the upper chord; (d) strain in long suspender.

5. Structural fatigue assessment

5.1. Corten-Dolan's model

On the basis of the Corten-Dolan's model [27], the fatigue damage D_d of the structural components under multi-level stress can be estimated from the fatigue damage under the maximum stress amplitude, expressed here as

$$D_d = \sum_{i=1}^{Nl} c_i r_i N_{fi}^b = c_{max} r_{max} N_{fmax}^b \tag{17}$$

where c_i is the number of damaged nuclei of the ith load level; r_i is the coefficient of damage propagation rate; N_{fi} is the cycle number of the ith stress level σ_i ($i = 1, Nl$); c_{max}, r_{max} and N_{fmax} are the maximum values of c_i, r_i and N_{fi}, respectively; b is the exponent coefficient of the fatigue damage; and Nl is the number of load levels.

The structural fatigue life under the multi-level loading condition is predicted by

$$N_s = \frac{N_{fmax}}{\sum_{i=1}^{Nl} \alpha_i (r_i / r_{max})^{1/b}} = \frac{N_{fmax}}{\sum_{i=1}^{Nl} \alpha_i (\sigma_i / \sigma_{max})^d} \tag{18}$$

where N_s is the total number of stress cycles under multi-level loading condition; σ_{max} is the maximum stress amplitude; α_i is the proportion of the stress cycle number under the ith stress level σ_i to the total stress cycle number with $\sum_{i=1}^{Nl} \alpha_i = 1$. The coefficient of damage propagation rate r_i is proportional to the stress level σ_i, and can be used for estimating the Corten-Dolan exponent parameter d.

Then, the relative fatigue damage D_i under multi-level stress can be defined as

$$D_i = \sum_{i=1}^{Nl} \frac{N_{fi} \alpha_i (\sigma_i)^d}{N_{fmax} (\sigma_{max})^d} \tag{19}$$

The Corten-Dolan exponent parameter d depends on many factors, such as material properties and non-linear loading conditions

[27]. The parameter d can be estimated from an exponential function of the stress state and stress cycle ratio [28], expressed here as

$$d = \exp\left[(n_i/N_i)^{\sigma_i/\sigma_{\max}}\right] + \varphi \tag{20}$$

where n_i denotes the stress cycle number of σ_i; N_i is the fatigue life under the constant stress amplitude σ_i; and φ represent a material-related parameter. To further consider the effect of stress ratio and stress interaction under multi-level loading, the parameter d in Eq. (20) are modified in [29] and [30].

5.2. Improved Corten-Dolan's model

The rail-cum-road bridge is subjected to highway vehicle loads and train loads. In comparison with train loads, the effect of highway vehicle loads is relatively small. To enhance the accuracy of fatigue assessment, an improved Corten-Dolan's model is proposed, which can be used for the bridge fatigue analyses to consider the interaction effect between highway vehicle loads and train loads. For the rail-cum-road bridge, the highway vehicle loads and train loads can be simplified as two different types of loads, and the fatigue damage of the bridge structural components N_z can be expressed as

$$N_z = \sum_{t=1}^{N_d} \frac{N_{\text{fmax}}\delta_o{}^{-1}}{\left[\vartheta_r(t) + \vartheta_v(t)(\sigma_v/\sigma_r)^{d_c}\right]} \tag{21}$$

where t is the bridge operation time; N_d is the expected service life of bridge; $\vartheta_r(t)$ is the ratio of stress cycles under the average daily train loads to the total stress cycles at time t; $\vartheta_v(t)$ is the ratio of stress cycles under the average daily vehicle loads to the total stress cycles at time t; δ_o is the amplification factor of the structural response under the combined effect of vehicle loads and train loads, and the maximum value of δ_o is typically taken as 1.2; and d_c is the modified exponent parameter related to stress history and material properties to better reflect the condition with multi-level traffic loads, defined here as

$$d_c = (\sigma_i/\sigma_{i-1})^h\left\{\exp\left[(n_i/N_i)^{\sigma_i/\sigma_{\max}}\right] + \varphi\right\} \tag{22}$$

where the power form of stress ratio $(\sigma_i/\sigma_{i-1})^h$ is adopted to consider the two consecutive load interaction effect, and the exponent parameter h can be taken as 2 or 3; and σ_i/σ_{i-1} is equal to unity when i =1.

Compared with the Miner's model, the improved Corten-Dolan's model can consider the coupling effect of highway vehicle loads and train loads, traffic load sequence and nonlinear accumulation of fatigue damage, which can be considered as an improved model for the fatigue analyses of the rail-cum-road bridge.

In general, the traffic volume increase rate is assumed to be a constant value, such as 0.1–0.5 % per year [34], which may not be consistent with the actual condition of the bridge due to traffic loads with territorial and random characteristics. The traffic carrying capacity of the bridge is related to the number of traffic lanes and the local economic conditions. Therefore, the traffic volume may not keep increasing at a constant rate during the bridge service life, and then it is reasonable to assume that the traffic volume tends to be saturated and stabilises gradually with the increase in bridge service time, while the vehicle weights keep unchanged in the future due to the enforced restrictions of vehicle weights.

The logistic growth curve can be adopted to model the S-shaped characteristics of the traffic volume growth behaviour [35]. At the initial stage, the logistic growth curve grows up approximately in an exponential form, then the growth rate slows down, and finally the growth rate vanishes. Based on the bridge traffic surveys [1], the modified logistic growth model for traffic analyses can be expressed as

$$N_r(t) = b_1 + Q_1/[1 - \delta_1\exp(-\nu_1 t)]; N_v(t) = b_2 + Q_2/[1 - \delta_2\exp(-\nu_2 t)] \tag{23}$$

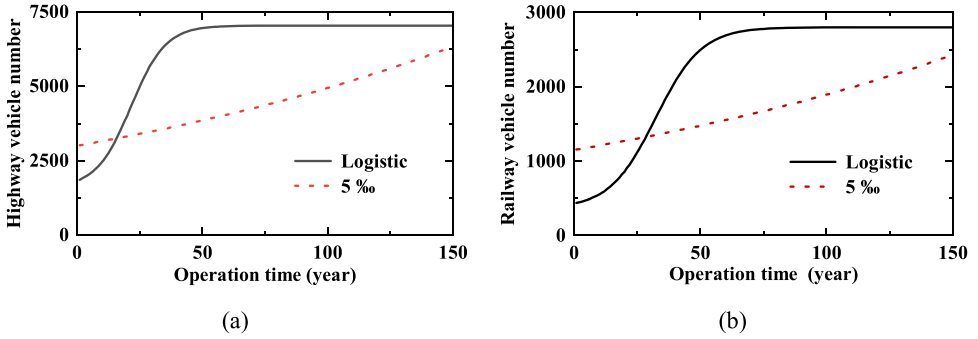

Fig. 11. Average daily traffic volume predictions based on the proposed logistic growth model and the constantly increasing rate (0.5 %): (a) highway vehicle volume; (b) train volume.

in which $N_r(t)$ and $N_v(t)$ are the numbers of the equivalent average daily traffic for railway and highway, respectively, and can be assumed to be constants over one year; b_1 and b_2 are the initial coefficients of railway and highway volumes, respectively; Q_1 and Q_2 are the maximum traffic coefficients of railway and highway, respectively; ν_1 and ν_2 are traffic growth parameters of railway and highway, respectively; δ_1 and δ_2 are the stabilisation parameters of railway and highway, respectively.

Fig. 11 presents the traffic prediction results from the proposed logistic growth model, which are compared with the predictions from the constant increase rate. From the results, highway and railway traffic volume predicted by the proposed logistic growth model are lower than those obtained from the constant increase rate of 0.5 % during the first 16 and 28 years, respectively. After that, the traffic volume predicted by the proposed logistic growth model become larger than those from the constantly increasing rate. The proposed logistic growth model indicates that the annual traffic volume increases exponentially between 17 and 34 years for highway, and between 29 and 46 years for railway. After these periods, the highway and railway traffic volume gradually reach stable stages. Thus, considering local economic development, the proposed logistic growth model appears more reasonable for traffic volume prediction.

5.3. Bridge fatigue assessment

The fatigue damage of the rail-cum-road bridge is mainly caused by the train loads and six-axle vehicle loads. Therefore, the multi-level traffic loads of the bridge can be simplified as a two-level stress spectrum. The equivalent stress amplitude under the traffic loads can be obtained from the measured data and numerical simulations. The ratios of the stress cycle numbers under the train loads $\vartheta_r(t)$ and under the six-axle vehicle loads $\vartheta_v(t)$ can be expressed, respectively, as

$$\vartheta_r(t) = \frac{N_r(t)N_r^e}{N_r(t)N_r^e + N_v(t)N_v^e};\ \vartheta_v(t) = \frac{N_v(t)N_v^e}{N_r(t)N_r^e + N_v(t)N_v^e} \tag{24}$$

where N_r^e and N_v^e are the numbers of equivalent stress cycles caused by a single train load or highway vehicle load passing over the bridge, respectively.

The measured strain can be decomposed using the wavelet packet method to eliminate low-frequency interferences from the ambient environment, such as temperature changes. The fatigue stress spectrum can be obtained by analysing the measured strain through the rain-flow counting criterion. The low-stress amplitudes (typically < 2 MPa) are generally caused by random interference, and the low-weight vehicles (typically < 3 t) can be ignored in the fatigue assessment due to less effect by lower stress levels. The number of limit fatigue stress cycles under a specific stress amplitude can be obtained from the *S-N* equation, namely

$$\log N = C - m\log\Delta\sigma \tag{25}$$

where $\Delta\sigma$ is the stress range; N is the number of stress cycles; C and m denote parameters depending on material properties, stress ratio and loading pattern. For the typical structural components of the rail-cum-road bridge, the values of $N = 10^7$, $\Delta\sigma = 64.1$ MPa, $C = 12.42$ and $m = 5$ could be adopted [25].

Moreover, the measured stress should be corrected by the modified Goodman's method, expressed here as

$$\sigma_a/\sigma_{a0} + \sigma_m/\sigma_u = 1/\mathrm{FoS} \tag{26}$$

where σ_a and σ_{a0} are alternating stress and fatigue limit stress, respectively; σ_m and σ_u are mean stress and ultimate tensile strength, respectively; and FoS represents the factor of safety, which is related to the shear strength and tensile static strength of the steel, typically taken as 0.58 for rail-cum-road bridges.

Due to the limited number of sensors and the complex structural system of the rail-cum-road bridge, it is difficult to obtain structural response of all critical components, such as the short suspenders and lower chords. From the updated finite element model of the rail-cum-road bridge, the fatigue stress spectrums of the critical structural components under traffic loads are obtained, which can be used for fatigue analyses. Based on the measured results and numerical simulation results, the equivalent stress amplitude and the daily stress cycles of the critical components are listed in Table 5, where σ_r^e and σ_v^e are the equivalent stress amplitudes under train loads and vehicle loads, respectively.

The cumulative fatigue damage caused by the traffic loads can be calculated by using the maximum stress amplitude and the equivalent number of stress cycles N^e [20], expressed as

$$N^e = N_t + \left(\frac{\sigma_{t1}}{\sigma_{tp}}\right)^m + \left(\frac{\sigma_{t2}}{\sigma_{tp}}\right)^m + \ldots + \left(\frac{\sigma_{ti}}{\sigma_{tp}}\right)^m \tag{27}$$

where N_t is the number of the maximum stress range due to a single traffic load; σ_{ti} are the higher-order stress range; and σ_{tp} is the primary stress range, calculated from the difference between the maximum and minimum stress ranges.

For the rail-cum-road bridge, the typical train loads are assumed to be the primary loads, and the six-axle vehicle loads are assumed to be the secondary loads. The cumulative fatigue damage of the bridge under two-level load conditions can be expressed as

$$D_c = \sum_{t=1}^{N_d} \delta_0 N_y t \left[\frac{N_r(t)N_r^e\left(\sigma_r^e\right)^{d_c} + N_v(t)N_v^e\left(\sigma_v^e\right)^{d_c}}{N_r^e\left(\sigma_r^e\right)^{d_c}}\right] \tag{28}$$

Table 5
Equivalent stress amplitudes of daily equivalent stress cycles.

Component	Measured data (MPa)		Component	Numerical prediction (MPa)	
	σ_r^e	σ_v^e		σ_r^e	σ_v^e
Upper H-shaped chord	66.61	27.09	Lower H-shaped chord	97.66	46.69
Long H-shaped suspender	82.33	45.49	Short H-shaped suspender	121.12	63.27
L/4 Arch ring	56.53	28.51	L/2 Arch ring	78.19	36.15

where N_y is the number of days in a year, taken as $N_y = 365$.

Fig. 12 gives the cumulative fatigue damage results of the short H-shaped suspender for different fatigue damage models, including the Miner's model, the Corten Dolan's model, and the proposed modified Corten Dolan's model. The results show that the fatigue damage obtained by the proposed model appears more significant than other models. When the bridge operation time reaches the design service life of 100 years, the cumulative fatigue damage is 0.25, 0.28 and 0.32 for the Miner's model, the Corten Dolan's model and the proposed model, respectively, which indicates that the short H-shaped suspender is not considered to have reached the end of the fatigue life. In the traditional fatigue analyses for the rail-cum-road bridge, the Miner's model is often adopted by ignoring the loading effect caused by highway vehicles. However, as shown in Table 1, the six-axle vehicles are overloaded significantly with a larger proportion of highway vehicle loads. The results in Fig. 12 indicate that the fatigue damage caused by the highway vehicle loads cannot be ignored in the rail-cum-road bridge fatigue analyses. By considering the combined effects of the multi-level traffic loads and selecting appropriately the exponent parameter d_c in Eq. (22), the cumulative fatigue damage of the proposed model appears more reasonable and reliable.

The critical components of the bridge, such as the lower H-shaped chord, short H-shaped suspender, and arch ring, are now selected for analysing the fatigue damage under traffic loads by using the improved Corten-Dolan's model. Fig. 13 shows the fatigue damage assessment results for the short H-shaped suspender by using different traffic prediction methods, including the proposed logistic growth model and the model with a constant increasing rate of 0.5 %. During the initial stage with 28 years of bridge service, the proposed logistic growth model shows low traffic levels and slow growth rates, and the fatigue damage increases gradually. Then, the cumulative fatigue damage for the proposed logistic growth model increases exponentially with the growth of the traffic volume. After 50 years of bridge operation, the difference in cumulative fatigue damage between the traffic predictions from the proposed logistic method and the constant rate method gradually becomes large. The results show that the structural fatigue damage under the constant traffic growth rate is lower than that from the proposed logistic growth model, and the short H-shaped suspender becomes more vulnerable under the traffic loads.

This study assumes that the bridge fatigue damage under the multiple loading condition is the same as the fatigue damage under the equivalent stress amplitude σ_f^e. The equivalent stress amplitude of the improved Corten-Dolan's model for the fatigue assessment of the rail-cum-road bridge can be calculated from

$$\sigma_f^e = \delta_o \left[\frac{N_r(t) N_r^e \left(\sigma_r^e\right)^{d_c} + N_v(t) N_v^e \left(\sigma_v^e\right)^{d_c}}{N_r(t) N_r^e} \right]^{1/d_c} \tag{29}$$

Based on the *S-N* curve and the improved Corten-Dolan's model, the limit state equation of the fatigue failure of the critical structural components of the bridge with consideration of traffic volume growth can be given as

$$g(t) = D_f - e_c D(t) = D_f - \frac{e_c N_d N_r(t) N_r^e \left(\sigma_f^e\right)^m t}{K_D} \tag{30}$$

where D_f is critical fatigue damage; $D(t)$ is the fatigue damage at bridge operation time t; e_c is the error correction factor of sensor

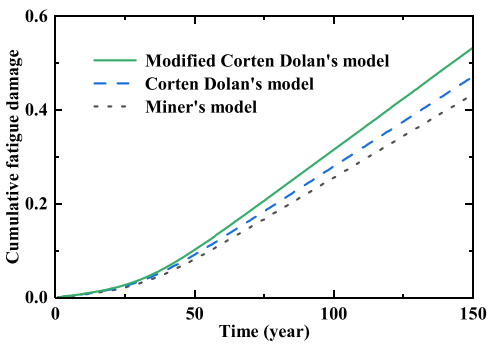

Fig. 12. Cumulative fatigue damage predicted by different models for the short H-shaped suspender.

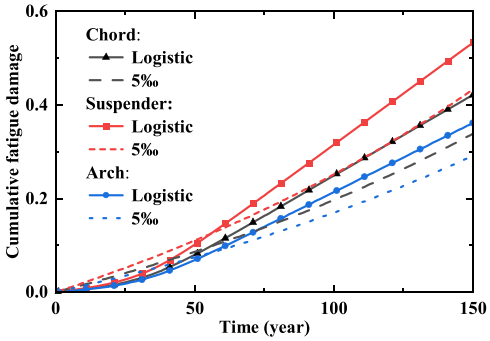

Fig. 13. Cumulative fatigue damage of the critical structural components for different traffic prediction models.

measurements or finite element model; and K_D is the fatigue strength coefficient. These parameters are assumed to be random variables following the lognormal distribution [36], as shown in Table 6.

From the limit state equation in Eq. (30), the fatigue failure probability of the critical structural components can be calculated from

$$P_f = P[g(t) < 0] = \widetilde{\Phi}\left(1 - \beta_f(t)\right) \tag{31}$$

where P_f is fatigue failure probability; β_f is fatigue reliability index depending on time t, for steel bridge typically $\beta_f = 2.0$–3.5 [36]; and $\widetilde{\Phi}$ is the standard normal distribution function.

Fig. 14 shows the results for fatigue reliability analyses of the critical structural components of the bridge, where the proposed modified Corten-Dolan's model is utilised. The Monte Carlo simulation method is adopted to calculate the fatigue reliability of the critical structural components with sampling number of 1,000,000. The results in Fig. 14 show that the fatigue reliability index decreases with the increase of bridge operation time, and the fatigue reliability index obtained from the proposed logistic growth model reduces more significantly than that from the constant rate model. The fatigue reliability index of the upper H-shaped chord, short H-shaped suspender, and arch ring reaches the target reliability index β_{target} of 3.0 after 60 years, 48 years, and 91 years of bridge service, respectively. The short H-shaped suspender is more vulnerable to fatigue failure under the combined cyclic traffic loads, as evidenced in regular condition inspections of the bridge.

6. Conclusions

This paper presents an effective method for the fatigue assessment of the rail-cum-road bridge from the SHM data. The measured data obtained from the installed SHM system on the bridge are analysed for traffic characteristics and modal identification. A three-dimensional finite element model is constructed and then updated by using the proposed regularised model updating method, and the updated numerical model is verified by using the measured dynamic response data. A realistic logistic growth model is proposed to simulate the growth of traffic volume, and then adopted for multi-level traffic load predictions. An improved Corten-Dolan's model is then proposed for the fatigue damage assessment of the critical structural components of the rail-cum-road bridge. From the obtained results, the following conclusions are noted:

a) From the SHM data, the probability distribution of traffic loads can be modelled using multiple Gaussian distributions, and the six-axle vehicles can be considered as the critical highway load model for the bridge fatigue assessment.
b) The proposed regularised finite element model updating method can provide better correlation between the numerical model and the associated actual bridge after the model updating from the measured natural frequencies. The verified numerical model can provide a reliable basis for evaluating the structural fatigue performance.

Table 6
Parameters of lognormal probability distributions for random variables.

Parameter	Description	Mean value	Unit	Coefficient of variation
D_f	Critical fatigue damage	1.00	-	0.30
e_c	Error correction factor	1.00	-	0.03
K_D	Fatigue strength coefficient	1.9×10^{15}	-	0.45
σ_f^e	Equivalent stress amplitude of upper H-shaped chord	100.76	MPa	0.17
	short H-shaped suspender	125.21	MPa	0.06
	arch ring	80.55	MPa	0.01

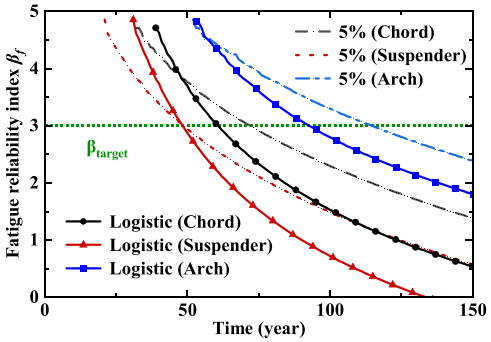

Fig. 14. Fatigue reliability index of various critical structural components from different traffic prediction models.

c) The proposed modified Corten-Dolan's model considers the non-linear fatigue damage accumulation and the coupled effects of train and highway vehicle loads. This approach yields more reliable assessments for structural fatigue damage and reliability analyses of the rail-cum-road bridge. Notably, the short H-shaped suspender, with its relatively short fatigue life, emerges as the most vulnerable component.

CRediT authorship contribution statement

Li Dai: Data curation. **Rosario Ceravolo:** Resources, Investigation. **Shou-Shan Lu:** Writing – review & editing, Writing – original draft, Visualization, Validation, Software, Formal analysis, Data curation. **Wei-Bin Wu:** Resources, Investigation, Data curation. **Hua-Peng Chen:** Writing – review & editing, Writing – original draft, Validation, Supervision, Resources, Project administration, Methodology, Funding acquisition, Conceptualization.

Declaration of Competing Interest

The authors declare that they have no known competing financial interests or personal relationships that could have appeared to influence the work reported in this paper.

Data Availability

Data will be made available on request.

Acknowledgements

The authors are very grateful for the financial supports received from the National Key Research and Development Program of China (Grant No. 2021YFE0105600 and 2023YFC3009400), the National Natural Science Foundation of China (Grant No. 51978263), the Key Project for Scientific and Technological Cooperation Scheme of Jiangxi Province (Grant Nos. 20212BDH80022 and 20223BBH80002), the Science and Technology Projects of Transport Department of Jiangxi Province (Grant Nos. 2021C0008 and 2022H0014).

References

[1] H.-P. Chen. Structural health monitoring of large civil engineering structures, John Wiley and Sons, New York, 2018.
[2] C.-R. Farrar, K. Worden, Structural health monitoring: a machine learning perspective, John Wiley and Sons, New York, 2013.
[3] J.-M. Ko, Y.-Q. Ni, Technology developments in structural health monitoring of large-scale bridges, Eng. Struct. 27 (12) (2005) 1715–1725.
[4] T.-H.-T. Chan, L. Guo, Z.-X. Li, Finite element modelling for fatigue stress analyses of large suspension bridges, J. Sound Vib. 261 (2003) 443–464.
[5] G.-D. Zhou, T.-H. Yi, W.-J. Li, J.-W. Zhong, J.-W. Zhang, Standardization construction and development trend of bridge health monitoring systerm in China, Adv. Bridge Eng. 1 (1) (2020) 1–18.
[6] D. Ribeiro, R. Calçada, R. Delgado, M. Brehm, V. Zabel, Finite element model updating of a bowstring-arch railway bridge based on experimental modal parameters, Eng. Struct. 40 (2012) 413–435.
[7] J.-E. Mottershead, M. Link, M.-I. Friswell, The sensitivity method in finite element model updating: a tutorial, Mech. Syst. Signal Process 25 (2011) 2275–2296.
[8] A. Sabamehr, C. Lim, A. Bagchi, System identification and model updating of highway bridges using ambient vibration tests, J. Civ. Struct. Health Monit. 8 (2018) 1–17.
[9] N. Debnath, A. Das, A multi-objective framework for finite element model updating using incomplete modal measurements, Struct. Control Health Monit. (2021) e2770.
[10] H.-P. Chen, N. Bicanic, Identification of structural damage in buildings using iterative procedure and regularisation method, Eng. Comput. (Swans.) 27 (8) (2010) 930–950.
[11] H.-P. Chen, T.-L. Huang, Updating finite element model using dynamic perturbation method and regularization algorithm, Smart Struct. Syst. 10 (4-5) (2012) 427–442.
[12] H.-P. Chen, K.-F. TEE, Structural finite element model updating using incomplete ambient vibration modal data, Sci. China Technol. Sci. 57 (9) (2014) 1677–1688.

[13] H.-P. Chen, T.-S. Maung, Regularised finite element model updating using measured incomplete modal data, J. Sound Vib. 333 (2014) 5566–5582.
[14] X. Zhou, C.-W. Kim, F.-L. Zhang, K.-C. Chang, Vibration-based bayesian model updating of an actual steel truss bridge subjected to incremental damage, Eng. Struct. 260 (2022) 114226.
[15] C. Fang, H.-J. Liu, H.-F. Lam, M.-O. Adeagbo, H.-Y. Peng, Practical model updating of the Ting Kau bridge through the MCMC-based bayesian algorithm utilizing measured modal parameters, Eng. Struct. 254 (2022) 113839.
[16] X.-W. Ye, Y.-Q. Ni, K.-Y. Wong, J.-M. Ko, Statistical analyses of stress spectra for fatigue life assessment of steel bridges with structural health monitoring data, Eng. Struct. 45 (2012) 166–176.
[17] Y.-Q. Ni, X.-W. Ye, J.-M. Ko, Monitoring-based fatigue reliability assessment of steel bridges: Analytical model and application, J. Struct. Eng. 136 (2010) 1563–1573.
[18] Z. Sun, J. Santos, E. Caetano, Data-driven prediction and interpretation of fatigue damage in a road-rail suspension bridge considering multiple loads, Struct. Control Health Monit. 29 (9) (2022) e2997.
[19] H.-Y. Gou, T.-Q. Zhao, S.-Q. Qin, X.-G. Zheng, A. Pipinato, Y. Bao, In-situ testing and model updating of a long-span cable-stayed railway bridge with hybrid girders subjected to a running train, Eng. Struct. 253 (2022) 113823.
[20] H. Tran-Ngoc, L.-Q. He, E. Reynders, S. Khatir, T. Le-Xuan, G. De Roeck, et al., An efficient approach to model updating for a multispan railway bridge using orthogonal diagonalization combined with improved particle swarm optimization, J. Sound Vib. 476 (2020) 115315.
[21] L. Deng, W.-C. Yan, L. Nie, A simple corrosion fatigue design method for bridges considering the coupled corrosion-overloading effect, Eng. Struct. 178 (2019) 309–317.
[22] Y.-S. Song, Y.-L. Ding, F. Jiang, Z.-W. Wang, J. Lu, H.-J. Jia, Multiaxial fatigue assessment for the hanger deck connection of a high-speed steel-truss-arch railway bridge, Appl. Sci. 11 (2021) 1142.
[23] P. Liu, H.-P. Lu, Y.-X. Chen, J. Zhao, L.-M. An, Y.-Q. Wang, et al., Fatigue analyses of long-span steel truss arched bridge part II: fatigue life assessment of suspenders subjected to dynamic overloaded moving vehicles, Metals 12 (2022) 1035.
[24] C.-S. Wang, P.-J. Zhang, G.-S. Wu, P.-Y. Li, Y. Wang, Fatigue damage evaluation of steel bridges considering thermal effect, Struct. Infrastruct. Eng. 18 (7) (2022) 1020–1033.
[25] X.-F. Guan, A. Giffin, R. Jha, Y.-M. Liu, Maximum relative entropy-based probabilistic inference in fatigue crack damage prognostics, Probabilistic Eng. Mech. 29 (2012) 157–166.
[26] Y. Liu, H.-P. Zhang, A.-M. ASCE, D.-R. Li, Y. Deng, N. Jiang, Fatigue reliability assessment for orthotropic steel deck details using copulas: application to Nan-Xi Yangtze River Bridge, Adv. Bridge Eng. 23 (1) (2018) 04017123.
[27] S.-P. Zhu, H.-Z. Huang, Y. Liu, L.-P. He, Q. Liao, A practical method for determining the Corten-Dolan exponent and its application to fatigue life prediction, Int. J. Turbo Jet. Engines 29 (2012) 79–87.
[28] H.-Y. Gao, H.-Z. Huang, Z.-Q. Lv, F.-J. Zuo, H.-K. Wang, An improved Corten-Dolan's model based on damage and stress state effects, J. Mech. Sci. Technol. 29 (8) (2015) 3215–3223.
[29] Q.-W. Xue, X.-Y. Du, An improved fatigue life prediction model based on loading sequence, Railw. Sci. 1 (1) (2022) 90–97.
[30] Q.-P. Liu, Y.-H. Gao, Y.-H. Li, Q.-W. Xue, Fatigue life prediction based on a novel improved version of the Corten-Dolan's model considering load interaction effect, Eng. Struct. 221 (2020) 111036.
[31] H.-P. Chen, Application of regularisation methods to damage detection in large scale plane frame structures using incomplete noisy modal data, Eng. Struct. 30 (2008) 3219–3227.
[32] X.-L. Yu, C.-M. Cheng, Y. Yang, M.-G. Du, Q.-B. He, Z.-K. Peng, Maximumly weighted iteration for solving inverse problems in dynamics, Int. J. Mech. Sci. 247 (2023) 108169.
[33] X.-Y. Lei. High speed railway track dynamics models, algorithms and applications, Springer Singapore, Singapore, 2022.
[34] K. Kwon, D.-M. Frangopol, Bridge fatigue reliability assessment using probability density functions of equivalent stress range based on field monitoring data, Int. J. Fatigue 32 (2010) 1221–1232.
[35] D. Kucharavy, Ruio R. De, Application of logistic growth curve, Procedia Eng. 131 (2015) 280–290.
[36] R. Helmerich, B. Kühn, A. Nussbaumer, Assessment of existing steel structures. A guideline for estimation of the remaining fatigue life, Struct. Infrastruct. Eng. 3 (3) (2007) 245–255.